ELSEVIER

Contents lists available at ScienceDirect

Journal of Controlled Release

journal homepage: www.elsevier.com/locate/jconrel





Polyphosphocholination of liposomic vehicles extends blood circulation, enhances cellular uptake, and lowers immunogenicity relative to PEGylation

Monika Kluzek ^{a,b,*}, Maryana Hamad ^a, Weifeng Lin ^{a,c}, Evgenia Mitsou ^{a,d}, Ziv Porat ^e, Yuri Kuznetsov ^f, Yaara Oppenheimer-Shaanan ^{a,g,h}, Jacob Klein ^{a,*}

- ^a Department of Materials and Interfaces, Weizmann Institute of Science, Rehovot 76100, Israel
- ^b IMol Polish Academy of Sciences; Warsaw 02-247, Poland
- c Key Laboratory of Bio-Inspired Smart Interfacial Science and Technology of Ministry of Education, School of Chemistry, Beihang University, Beijing 100191, PR China.
- ^d Institute of Chemical Biology, National Hellenic Research Foundation, 11635 Athens, Greece
- ^e Flow Cytometry Unit, Life Sciences Core Facilities, Weizmann Institute of Science, Rehovot 76100, Israel.
- f Department of Veterinary Resources, Weizmann Institute of Science, Rehovot 76100, Israel
- g Department of Plant Pathology and Microbiology, The Institute of Environmental Science, The Robert H. Smith Faculty of Agriculture, Food, and Environment, The Hebrew University of Jerusalem. Rehovot. Israel
- ^h Department of Life Sciences, Achva Academic College, Arugot 79804, Israel

ARTICLE INFO

Keywords: Liposomic delivery vehicles Polyphosphocholinated liposomes PEGylated liposomes Blood circulation Immune response

ABSTRACT

Intravenous liposomal drug delivery holds great promise for pharmaceutical efficacy, but faces challenges such as rapid clearance and immune system degradation. PEG-based liposome surface functionalization (PEGylation), currently the gold-standard and most widely-used approach to address these issues, is prone to reduced cellular uptake and accelerated bloodstream clearance (ABC) effect upon repeated administration due to immune activation. We demonstrate a novel liposome surface functionalization using poly(2-methacryloyloxyethyl phosphorylcholine) (pMPC) that significantly overcomes these limitations while maintaining comparable colloidal stability. Such polyphosphocholinated liposomes exhibit tunable cellular uptake, and prolonged blood circulation times, both modulated by polymer length, alongside reduced immunogenicity (lower IgM antibody elicitation) and a diminished ABC effect compared to PEG-liposomes. These polymer-length-dependent properties offer flexibility in optimizing drug delivery systems, positioning pMPCylated liposomes as a compelling alternative to PEGylated formulations with clear advantages for liposomal drug delivery therapeutics.

1. Introduction

Engineered drug nanocarriers have shown significant potential in treating a range of diseases including cancer [1], bacterial [2], and recently viral infections [3]. Over the years, a broad variety of organic and bio-inspired materials [4] have been proposed for drug delivery [5] including nanoparticles [4,6,7], polymeric [8–10] and protein derivatives [11]. Among these, liposomes, characterized by their lipid-membrane-enclosed vesicular structure capable of encapsulating a wide range of compounds [3,12,13], have been extensively studied and used as versatile delivery vehicles for a range of clinical applications [14]. However, the *in vivo* drug delivery performance of such carriers is limited by a number of factors [15]. Upon intravenous (IV)

administration, liposomes interact with a diverse array of proteins, resulting in the formation of a "protein corona" layer on their surface [16–18] that not only limits their blood circulation [16] but also controls their cellular interactions and biodistribution [19,20]. The presence of such a corona renders liposomes more prone to opsonization, leading to their rapid clearance [16] by the innate immune system [21,22] and, consequently, a loss of therapeutic efficacy [23].

A common strategy to minimize such limitations is to attach nonionic, hydrophilic polymers to the liposome surfaces, with polyethylene glycol (PEG) being the most widely-used one ('gold standard') [24,25]. PEGylation of liposomes selectively suppresses nonspecific protein adsorption by blocking the protein-binding sites [26,27], thereby extending their circulation half-life [28,29]. As a result of

E-mail addresses: m.kluzek@imol.institute (M. Kluzek), jacob.klein@weizmann.ac.il (J. Klein).

^{*} Corresponding authors.

prolonged circulation, PEG-liposomes are able to accumulate at the target site and deliver their cargo more efficiently. The success of PEGliposomes has a well-established history in drug delivery and has reached clinical maturity [30]. However, PEGylation is also associated with significant limitations [25], including reduced cellular uptake [31-33] and the triggering of an immunological response [34,35]. Indeed, recent studies have reported that a single intravenous injection of PEG-liposomes into different animal species induces the production of PEG-reactive IgM [36,37] and IgG [35] antibodies and activates the complement system [38,39], resulting in the rapid clearance of PEGylated liposomes upon subsequent administration [40]. This phenomenon, known as the accelerated blood clearance (ABC) effect [38,41], can alter the biodistribution of nanocarriers and compromise the efficacy of PEG-liposomal carriers, particularly in the context of repeated administration for chronic conditions [25,37,42]. Additionally, PEG-liposomes may stimulate the complement system [38,43], with approximately 7 % of individuals exposed to PEG developing antibody levels capable of inducing anaphylactic reactions [44]. Given these limitations of PEGylation, there is growing interest in developing alternative liposome surface functionalizations. A promising candidate being investigated is the use of polyzwitterions [45].

These polymers, encompassing both positively and negatively charged groups, have shown promise in resisting the formation of anti-polymer antibodies [46,47], thereby increasing blood circulation and enhancing therapeutic efficacy [48,49]. By evading the induction of an immune response, polyzwitterion-functionalized liposomes hold promise as an effective.

alternative to PEGylation [50].

In this study, we present an innovative zwitterionic approach to liposomal functionalization using poly(2-methacryloyloxyethyl phosphorylcholine) (pMPC) [51,52]. This polymer has been shown to prolong the plasma circulation time of encapsulated proteins [53] and conjugated DNA aptamers [54]. It has also been successfully implemented in clinical settings for coating medical devices [55], where it suppresses biological reactions and demonstrates blood compatibility [56]. Adler et al. [57] demonstrated that pMPC surface functionalization can reduce the adsorption of proteins and antibodies due to the hydration shell formed by the polymer. Earlier work from our lab demonstrated the potential of pMPC for therapeutics and drug delivery, with pMPCylated liposomes applied in osteoarthritis treatment [51,58] and to enhance drug carrier affinity for bacterial biofilms [59]. This study builds on that work by validating the effects of pMPCvlation on liposomal carriers' cellular uptake, in vivo pharmacokinetics, and immunogenic profiles, laying a foundation for its clinical applications.

We now investigate the potential of pMPC-based liposome functionalization for clinical applications, in particular drug delivery via liposomic vehicles, by probing the effects of polymer chain length and surface coverage on two key factors for carrier's efficacy, i.e. blood circulation time and payload delivery. The persistence of carriers in the bloodstream, reflective of effective dosage and requirement for multiple administrations, was quantified in vivo by measuring presence of fluorescently labeled liposomes in the blood of murine models at various time points. Similarly, we probed indirectly the payload delivery of fluorescently labeled carriers in vitro by quantifying cellular uptake using imaging flow cytometry. Direct comparison reveals that pMPCfunctionalized carriers outperform commercially employed PEGylated liposomes in key parameters. pMPCylation offers greater flexibility and superior overall properties, with longer pMPC chains exhibiting enhanced bloodstream retention and shorter pMPC chains demonstrating improved cellular uptake compared to their PEG counterparts, enabling optimization of functionalization through the judicious selection of chain lengths. Moreover, pMPC-functionalized liposomes elicit significantly lower immunogenic responses in vivo compared to PEG, with reduced IgM antibody production in mice. The observed decrease in IgM antibodies further translates to a significantly lower susceptibility to ABC effect upon repeated administration. By addressing this major

limitation of current PEGylated liposomes, pMPC-functionalized carriers present a promising solution for maintaining consistent treatment across multiple doses.

2. Materials

HSPC (Hydrogenated soybean phosphatidylcholine, Mw 786.11), Stearylamine (CH3(CH2)17NH2, Mw 269.509, Cat. No. 305391), 18:0 PEG5000 PE (1,2-distearoyl-sn-glycero-3-phosphoethanolamine-N-[methoxy(polyethylene glycol)-5000] (ammonium salt), Mw 5801.071, Cat. No. 880520P), 18:0 PEG2000 PE (1,2-distearoyl-sn-glycero-3-phosphoethanolamine-N-[methoxy(polyethylene glycol)-2000] (ammonium salt), Mw 2790.521, Cat. No. 880120P), were purchased from Sigma-Aldrich (Rehovot, Israel). mPEG-DSPE, MW 10 k, Cat. No. PSB-2043) was purchased from Creative PEGWorks (Chapel Hill, NC, USA). RPMI media (Cat. No. 11875093, Gibco), fetal bovine serum (FBS, Cat. No. A5256701, Gibco), penicillin-streptomycin (10,000 U/mL, Cat. No. 15140122, Gibco), DiI Stain (1,10-dioctadecyl-3,3,30,30-etramethylindocarbocyanine perchlorate C59H97ClN2O4, Cat. No D3911) and Vybrant DiD Cell-labeling solution (Cat. No V22887) were provided by Thermo Fisher Scientific (Waltham, MA, USA), 16 % aqueous solution of formaldehyde (Cat. No 15700) was provided by Electron Microscopy Science (Hatfield, PA, USA). Mouse IgM ELISA kit (Cat. No. ab133047) was purchased from Abcam (Cambridge, UK).

3. Methods

3.1. Liposome preparation (LUVs) and characterization

HSPC, pMPC (2 kDa /5 kDa /10 kDa / 20 kDa, 2 % or 5 % mol/mol) or HSPC / PEG (2 kDa /5 kDa/ 10 kDa, 2 % or 5 % mol/mol) were dissolved in chloroform or chloroform/methanol mixture (2:1) and organic solvent was evaporated using first nitrogen stream, followed by vacuum pumping. For introducing a positive charge into liposomes, 5 % (mol/mol) of stearylamine (SA) was added in chloroform before evaporation. The lipid film was then hydrated with PBS (1×, osmol = 280 mOsmo/kg) at 70 °C to reach the desired concentration. The resulting multi lamellar vesicle (MLV) suspensions were sonicated for 15 min at 70 °C to disperse larger aggregates. The vesicles were subsequently downsized by extrusion (Lipex, Northren Lipids Inc.,Canada) through 400 nm and 200 nm polycarbonate membrane. The extrusion was performed 11 times through each membrane at 65 °C.

The size and $\zeta\text{-potential}$ of the liposomes was measured with a ZetaSizer Nano ZS (Malvern Instruments, UK) at 25 °C. Triplicate measurements with a minimum of 10 runs were performed for each sample.

To ensure a consistent amount of injected liposomes, nanoparticle tracking analysis (NTA) measurements were performed. Samples were diluted with PBS to a final volume of 1 mL. Optimal dilution for each sample was found by pre-testing the sample until ideal particle-perframe value (20–100 particles/frame) was obtained. For each measurement, five 1 min videos were captured at 25 $^{\circ}\text{C}$, with at least 300 μL displacement between each video. The number of completed tracks in NTA (Malvern NanoSight NS300, Malverin, UK) measurements was always greater than the proposed minimum of 1000 in order to minimize data skewing based on single large particles.

3.2. Cell culture

Vero cells were cultured in RPMI medium, supplemented with 1 % Pen/Strep and 10 % fetal bovine serum (FBS). Cells were maintained at 37 $^{\circ}\text{C}$ in a humidified atmosphere of 95 % air and 5 % CO₂.

3.2.1. Evaluation of cytotoxicity

Liposomes cytotoxicity was determined by the production of the yellow formazan product upon cleavage of XTT by mitochondrial

dehydrogenases in viable Vero cells. The cells were seeded onto 96-well plates (4 \times 10^4 cells/well) in RPMI media. When the confluent state was reached (usually after 24 h), 50 μL of pMPC-, PEG- liposomes in PBS solutions were then added. After 24 h incubation, the cells were incubated with 50 μL of XTT solution for 3 h. Absorbance values were later measured with a multiwell-plate reader (Cary 100 Bio, Varian Inc., USA) at a wavelength of 450 nm. Background absorbance was measured at 620 nm and subtracted from the 450 nm measurement. The experiments were repeated at least three times, and six replicates were prepared for each liposomal concentration tested in every experiment. A solution of in liposome- free RPMI medium was used as a positive control.

The potential toxic effect of the different liposomal formulation tested was expressed as a viability percentage calculated using the following formula:

%Viability = $100 - [(ODtest/ODc) \times 100]$.

Where ODtest was the optical density of those wells treated with the liposome solutions, and ODc was the optical density of those wells treated with liposome-free RPMI media.

3.2.2. Fluorescence confocal microscopy visualization

Vero cells were seeded at 10^5 density of cells per well in glass bottom dish (35 mm dish with 14 mm bottom well, Cellvis (USA)). After 24 h, medium was changed and liposome solution was added (final concentration 0.2 mM), and samples were incubated for 4 h at 37 °C (95 % air and 5 % CO₂). 30 min before end of incubation 0.8 μ L of DAPI (10 mg/mL) was added in each dish. Following incubation, cells were carefully washed minimum 5 times with sterile PBS. Subsequently, cells were fixed using 4 % formaldehyde for 15 min at 37 °C. After fixation, cells were washed thoroughly with sterile PBS and 10 μ L of Vybrant DiD was added into each sample for 10 min at 4 °C. Cells were washed and 2 mL of PBS was added. Samples were visualized using Axioplan2 microscope (ZEISS, Germany) equipped with ORCA Flash 4.0 camera (HAMA-MATSU). Image processing was performed using ImageJ software (USA).

3.2.3. ImageStream measurements

Vero cells were seeded into 6-well plate with density of 10⁶ cells / well. After 24 h, medium was changed and liposomal solution was added (final concentration 0.2 mM), and samples were incubated for 4 h at $37\,^{\circ}\text{C}$ (95 % air and 5 % CO₂). Following incubation, cells were washed with sterile PBS and 0.25 % Trypsin was added (3 min, 37 °C (95 % air and 5 % CO₂)). After incubation, cells were detached and resuspended in medium by gentle pipetting. Suspension was centrifuged at 400 g for 5 min, supernatant was discarded and pallets were resuspended in fresh medium following another round of centrifugation. Final pellets were resuspended in 35 µL of sterile PBS. Cells were imaged using multispectral imaging flow cytometry (ImageStreamX mark II imaging flowcytometer; Amnis Corp, Seattle, WA, part of Cytek). Approximately $1.5-2.0 \times 10^4$ cells were collected from each sample and data were analyzed using image analysis software (IDEAS 6.3; Amnis Corp). Data were acquired using a \times 60 lens (NA = 0.9), and lasers used were 405 nm (120 mW) and 561 nm (40 mW). Single stained controls were acquired to calculate the dye spillover matrix between channels. Data were analyzed using the manufacturer's software IDEAS 6.2 (AMNIS corp.). Cells were first gated according to their area (in µm²) and aspect ratio (the Minor Axis divided by the Major Axis of the best-fit ellipse) of the brightfield image. Cropped cells were eliminated using the bright-field Area and Centroid X (the number of pixels in the horizontal axis from the upper, left corner of the image to the center of the mask) features. Cells were further gated for DiI staining according to its corresponding intensity. Plotting these features on a bi-variate plot gave a clear distinction of the liposome internalization (Fig. S3).

3.3. Animal care and blood circulation kinetic measurements

All mice were housed in groups of 2-5 mice per micro-isolator cage in a room with a 12 h light/dark schedule with free access to food and water. Eleven-week-old female Hsd:ICR (CD1) mice were purchased from Envigo (Israel). DiI- labeled liposomes suspension (100 µL, 5 mM) was administered (IV) intravenously (lateral tail vein) and at well-define time points blood was collected from facial vein into test tubes for serum collection (KABE LABORTECHNIK GmbH. (Germany)). Tubes were centrifuge at 1000 g for 10 min (4 $^{\circ}$ C), and 10 μ L of serum was collected and exanimated for DiI presence using microplate reader (BMG LAB-TECH GmbH, Germany). 24 h post injections mice were euthanized in their home cages by exposure to carbon dioxide and organs were collected. Further, organs were homogenized in 2 mL PBS and 2 mL of chloroform was added followed by 2 days shake at 4°C. Organic phase was extracted, evaporated and sample was resuspended in 110 µL of ethanol. The DiI content was measured using microplate reader (BMG LABTECH GmbH, Germany).

3.3.1. Blood circulation times and accelerated blood clearance (ABC)

Liposomes suspension (100 μ L, 0.01 μ mol phospholipid/kg) was administered intravenously (IV) (lateral tail vein). Five days postinjection another dose of DiI-labeled liposomes (100 μ L, 0.05 μ mol phospholipid/kg) were injected *via* tail vein and at well-define time points blood was collected from facial vein into test tubes for serum collection (KABE LABORTECHNIK GmbH. (Germany)). Tubes were centrifuge at 1000 g for 10 min (4°C), and 10 μ L of serum was collected and exanimated for DiI presence using microplate reader (BMG LABTECH GmbH, Germany). The circulation half-time was determined by exponentially fitting the raw data using OriginJ software, version 1.52i (NIH, USA), as shown in Fig. S6.

3.3.2. Toxicity assessment of repeated injections (IV and IP) of pMPC-liposomes

IV injections: $100~\mu L$ of functionalized liposomes (10~mg/kg BW) was injected into the lateral tail vein of eleven-week-old female Hsd:ICR (CD1) mice. The injection was held upon heating the tail with a lamp in order to dilate the vessels followed by tail swabbing with 70 % alcohol. PBS or liposomal solution were slowly injected using 1 mL syringe with 27Gx1/2 needle. Injections were done 3 times per week for 9 days. IP injections: $100~\mu L$ of liposomes (10~mg/kg BW) was IP-injected into eleven-week-old female Hsd:ICR (CD1) mice using U-100 insulin syringes. Injections took place 5 times per week for 9 days. All mice used in the study were carefully monitored for any clinical signs and distress and weight was recorded on a daily basis.

3.3.3. IgM levels in mouse serum

Functionalized liposomes were intravenously injected \emph{via} the tail vein into CD1 mice at a dose of 0.01 μ mol phospholipid per kg. Serum IgM levels were measured five days post-injection using the ELISA kit from Abcam (ab133047) following the manufacturer's recommendations.

3.4. Statistical analysis

All statistical assays performed were analyzed using Analysis of Variance (ANOVA) and then Tukey's test using OriginJ software v1.52i (NIH, USA). *P*-values <0.05 were considered statistically significant.

4. Results and discussion

4.1. Colloidal stability of pMPCylated liposomes vs. PEGylated liposomes in serum-enriched medium

The pMPC-distearoylphosphatidylethanolamine (pMPC-DSPE) conjugate, first described in ref. [52], was used to functionalize liposomes,

for comparison with the current gold-standard PEG-DSPE [60,61]. We prepared large unilamellar vesicles (LUVs) with an average diameter of approximately 180 nm (Table S1) composed of HSPC with either 2 % or 5 % (mol/mol) PEG or pMPC of varying polymer lengths (ranging from 2 kDa to 20 kDa). As the presence of functionalized DSPE results in a negatively charged carrier membrane, which has been reported to be more prone to activate the complement system by triggering the classical pathway [62,63], we also doped the liposomes with an equivalent fraction of the positively charged stearylamine (SA). Interestingly, pMPC-LUVs exhibited a chain-length-dependent modulation of surface charge. We attribute this as follows. Whereas shorter polymer chains (\leq 5 kDa) allowed the cationic signature of SA to dominate at the corona/solution slip plane, yielding near-neutral or positive zeta potentials, longer chains (10-20 kDa) established a more extended hydrated corona that masked the SA contribution at this slip plane, presumably due to electrostatic screening over the thicker coronas. Since, as is established in prior work on phosphorylcholine-based zwitterionic surfaces [64], and in recent studies on pMPC coatings and their influence on nanoparticle charge profile [65], the outer corona surface has a negative potential (due to the phosphocholine groups of the pMPC chains), the result is a net positive zeta potential for the thinner coronas and a neutral or net negative zeta potential for the thicker coronas (Table S1). This interfacial effect highlights the unique capacity of extended pMPC coronas to shield embedded cationic components and tune electrostatic interactions, as established.

The resulting pMPC-LUVs display long-term colloidal stability in PBS solution (72 h), indicated by the hydrodynamic diameter and polydispersity index (PDI) measured *via* dynamic light scattering (DLS, Fig. 1 and Table S1) and excellent biocompatibility profile (Fig.

S1) at any polymer length, similar to PEG-LUVs (Figs. 1, S1 and Table S1). To check whether a protein corona would form under physiological conditions, we probed the size distribution of liposomes incubated for 72 h at 37 $^{\circ}$ C in cell culture medium supplemented with 10 % fetal bovine serum (FBS).

PEG-LUVs show no aggregation at any probed polymer length (Fig. 1C, Table S1). For pMPC-LUVs, the shortest polymers (pMPC 2 kDa) display clear aggregation (multiple peaks at higher hydrodynamic diameters and PDI ≥ 0.25) at both grafting percentages (Fig. 1A, Table S1) suggesting that such surface functionalization length is insufficient to prevent corona formation. Size distribution of the same carriers in the absence of SA, where the presence of additional negative charge would provide electrostatic repulsion, still shows aggregation, indicating that the poor colloidal stability is due to the polymer being too short (Fig. 1A); we recall that 2 kDa pMPC has about 6 monomers compared with ca. 45 monomers for 2 kDa PEG, so this finding is not

surprising. Conversely, pMPCylated carriers with increasing polymer molecular weights (5 kDa, 10 kDa, and 20 kDa) displayed good long-term colloidal stability, comparable to that of PEGylated LUVs (Fig. 1B and C), consistent with previous reports [66].

4.2. Effect of pMPC length on cellular uptake

We evaluated the impact of pMPCylation on cellular uptake using Vero cells, a robust and common model utilized both for viral infections and antiviral treatments [67–69], and nano-compounds internalization [70,71]. Since the goal of this study was to first demonstrate the immunological and pharmacokinetic advantages of pMPC-liposomes, we focused here on the total internalization of pMPCvlated carriers over long incubation time, reserving detailed characterization of pMPC impact on uptake kinetics, subcellular localization, and cellular specificity to future studies. Cells were incubated with DiI-labeled liposomes (final concentration: 0.2 mM) functionalized with varying lengths of pMPC (5, 10 and 20 kDa) or PEG (2, 5 and 10 kDa). After thorough washing to remove non-internalized liposomes, the cells were analyzed using ImageStream flow cytometry to quantify the total amount of fluorescence arising from DiI on each cell (Fig. S2), as a proxy for total amount of liposomes internalization by cells independently of entry or uptake route, or specific sub-cellular localization.

As shown in Fig. 2, PEG-functionalized carriers showed similar uptake at 2 and 5 kDa, with a decrease observed only at 10 kDa. In contrast, pMPC-functionalized liposomes exhibited a clear inverse relationship between polymer length and uptake, with 20 kDa pMPC showing over 20-fold lower uptake than 5 kDa pMPC. Notably, at 5 kDa, pMPC-liposomes demonstrated significantly higher uptake compared to 2 kDa PEG-liposomes while maintaining similar colloidal stability (Fig. 1). The uptake of PEG carriers can be attributed to steric repulsion, leading to limited interaction with cell surfaces. As PEG molecular weight increases to 10 kDa, steric hindrance becomes significant enough to substantially impair the carrier's ability to interact with cell membranes [72].

In contrast, pMPC-LUVs display a more complex interaction pattern, suggesting a balance between repulsion and affinity for cell membranes. Indeed, pMPC has been proposed to have a high affinity for scavenger receptors that are expressed on cells, promoting internalization *via* endocytosis [73–75]. This strong affinity of 5 kDa pMPC-LUVs is further evidenced by high cellular uptake, even at reduced SA content (2 % or 0 % mol/mol) and increased electrostatic repulsion (Fig. S4). The negative charges present on most cell membranes would typically increase electrostatic repulsion with negatively charged liposomes, potentially impairing uptake. However, even under these unfavorable conditions,

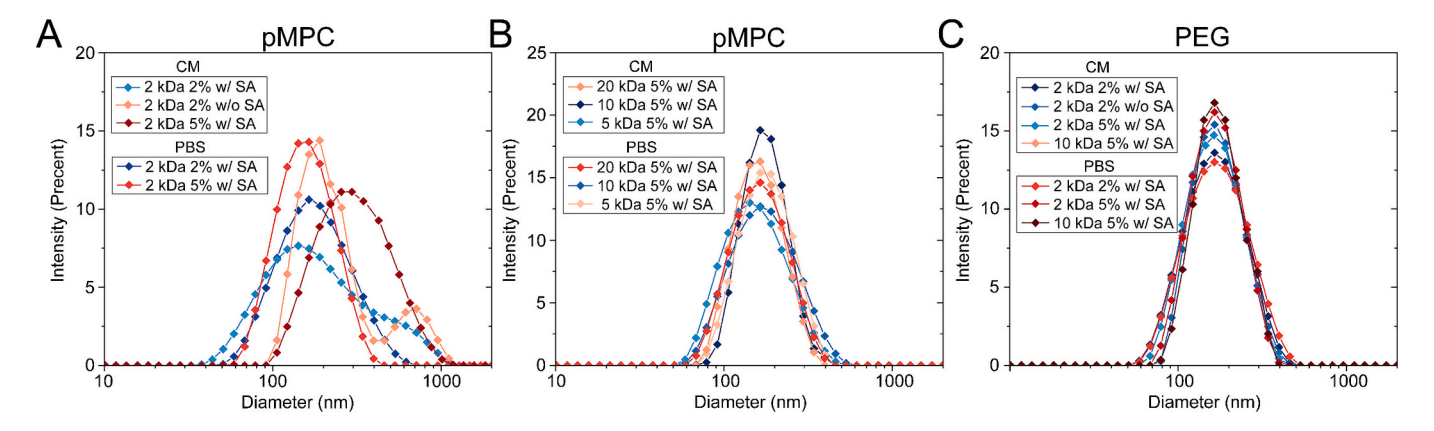


Fig. 1. Changes in hydrodynamic diameter of functionalized liposomes (pMPC- or PEG-) with various polymer lengths and grafting percentages incubated in PBS or cell medium (CM) supplemented with 10 % fetal bovine serum (FBS) for 72 h at 37 °C. (A) pMPC-liposomes with 2 kDa chain length at 2 % and 5 % grafting percentages; with (w/) or without (w/o) 5 % (mol/mol) SA (B) pMPC-liposomes with higher chain lengths (5 kDa, 10 kDa and 20 kDa) at 5 % grafting percentage, with (w/) 5 % (mol/mol) SA. (C) PEG-liposomes at 2 kDa and 10 kDa chain length with 2 % or 5 % grafting percentages; with (w/) or without (w/o) 5 % (mol/mol) SA. A complete list of DLS run results is presented in Table S1.

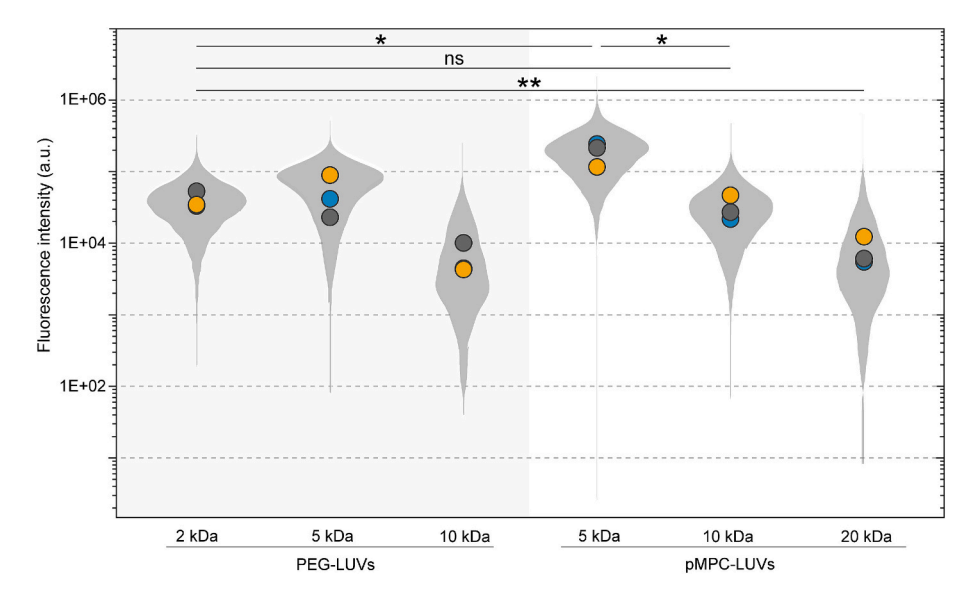


Fig. 2. Quantified cellular uptake of DiI-labeled liposomes, doped with 5 % (mol/mol) SA and functionalized with 5 % (mol/mol) pMPC- or PEG- with increasing chain length obtained from ImageStream analysis (gating strategy and data analysis are presented in Fig. S3). Data are shown as a violin plot reflecting data distribution from three biological replicates, with a filled circle indicating the median of each dataset. Values are plotted on a log10 scale. The number of cells collected per tested condition is \geq 1500. *P*-values obtained by one-way ANOVA performed on medians extrapolated from each biological repeat. Statistical significance: *p < 0.05, **p < 0.01, **** p < 0.001, **** p < 0.0001, ns – not significant. A summary of confidence values is listed in Table S2.

pMPC-LUVs demonstrate significant cellular uptake, indicating a strong affinity between MPC moieties and cell surfaces (Fig. S4).

The observed decrease in cellular uptake with increasing pMPC polymer length may be attributed to a balance between steric repulsion and molecular affinity. This phenomenon aligns with reports on MPC polymersomes [74], where binding to the first exposed MPC unit is highly favorable, but subsequent interactions with moieties buried within the polymer brush encounter increasing steric repulsion. Thus, for shorter pMPC chains, the interaction with specific scavenger receptors enhances the cellular uptake, while for longer pMPC chains, steric repulsion overcomes this effect [76]. This mechanism allows for fine-tuning of carrier uptake based solely on pMPC molecular weight, offering either enhanced or comparable internalization to PEGylated vehicles, depending on specific requirements.

Furthermore, visualization of the carriers binding and internalization by cells using confocal microscopy (Fig. 3) demonstrates that both pMPC (Fig. 3C) and PEG (Fig. 3B) carriers enter cells *via* endocytosis, consistent with pMPC interacting with scavenger receptors on the cell surface, characterized by the localized point-like distribution of the DiI fluorescent signal otherwise absent in untreated cells (Fig. 3A). This is further validated by the intracellular localization of such puncta (Fig. 3D), which rules out liposomes bound to or fused with the cell membrane.

4.3. Impact of pMPC length on liposome blood circulation time

After evaluating the role of pMPC polymer length on *in vitro* cellular uptake, we assessed how pMPC affects its carriers' circulation profile *in vivo*. First, we examined the toxicity of repeated administration of pMPC- or PEG-functionalized liposomes for potential multi-dose treatments. Adult CD1 mice were injected intraperitoneally (IP) (Fig. S5A) or intravenously (Fig. S5B) with 10 mg/kg liposomes for a total of 10 (IP) or 6 (IV) injections over a period of 9 days. During the experiment, we monitored the mice's body weight daily, as the significant variations above 20 % can indicate toxicity [77].

At the end of the experiment, all injected groups showed an increase in body weight for both IP and IV injections (Fig. S5). In all tested groups, there were no significant differences in body weight between liposome-treated and control mice (p > 0.05). Furthermore, no mortality was observed among mice exposed to repeated doses of liposomes, whether functionalized with pMPC or PEG, bearing net negatively charged membranes, or doped with SA. No additional visible signs of toxicity were observed in mice treated with liposomes, specifically, there were no changes in fur appearance, eyes, sleep cycles, salivation, food or water intake, or other visible signs of distress. The obtained results highlight the safety of pMPCylation for their potential use as drug carrier functionalization even at prolonged administration.

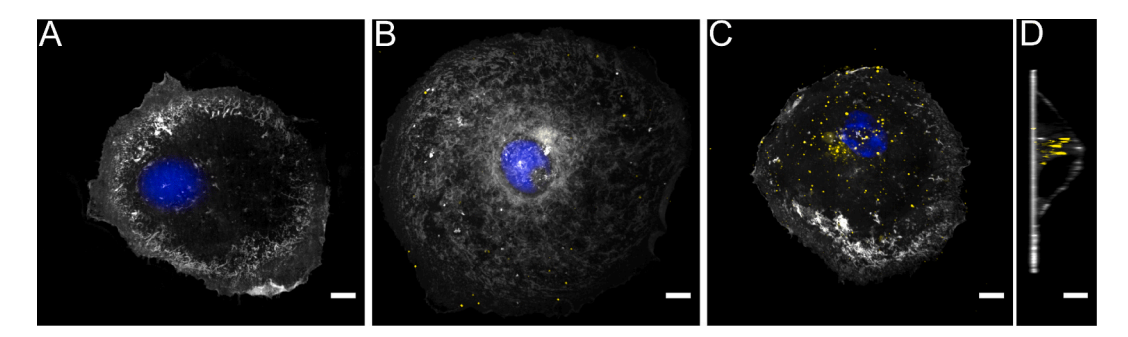


Fig. 3. Representative confocal microscopy images of uptake of DiI-labeled (yellow) liposomes, functionalized with 5 % (mol/mol) pMPC (5 kDa) or PEG (2 kDa) and doped with 5 % (mol/mol) SA, by Vero cells after 4 h incubation at 37 °C. (A) non-treated (B) PEG-LUV; (C) pMPC-LUVs (D) Orthogonal section of (C). Cell membranes are stained with Vybrant DiD (gray), and nuclei with DAPI (blue). Scale bar: 10 μm. (For interpretation of the references to colour in this figure legend, the reader is referred to the web version of this article.)

We then investigated the impact of pMPC vlation on blood circulation kinetics and biodistribution. DiI-labeled liposomes were injected via tail vein into CD1 mice at 5 mM (12.25 mg/kg body weight), with blood samples collected at specific time points to measure fluorescence signals. As a negative control, we employed carriers functionalized with 2 kDa pMPC, which showed significant aggregation in protein-rich medium (Fig. 1). These vehicles exhibited a short half-life of approximately 0.1 h, providing a reference for fast elimination from the bloodstream, as shown in Fig. 4B and C. Analysis of blood circulation kinetics revealed distinct patterns for PEG- and pMPC- functionalized liposomes across various molecular weights (Fig. 4A, B). Both PEG (2, 5 and 10 kDa) and pMPC (5, 10 and 20 kDa) demonstrated longer clearance times, with half-lives of at least 2 h for all systems probed. However, while PEGylation showed no correlation between molecular weight and blood circulation, with all three polymer lengths having similar blood elimination half-lives of approximately 2.5 h, the pMPCylated carriers demonstrated a clear dependence on polymer length. The shortest pMPC (5 kDa) had a lifetime comparable to PEG, which increased with longer pMPC polymers, reaching 4.1 \pm 0.3 h at 20 kDa.

The significant disparities in blood circulation kinetics between PEG and pMPC (Fig. 4C, D), despite comparable colloidal stability, highlight the unique polymer-length-dependent properties of pMPC-liposomes. The zwitterionic structure of pMPC likely enhances surface hydration and steric shielding, reducing non-specific protein adsorption and contributing to prolonged circulation times with increasing molecular weight, reaching 4.1 \pm 0.3 h for 20 kDa pMPC compared to $\sim\!2.5$ h for PEG across all tested lengths (2, 5, and 10 kDa). Notably, 40 kDa pMPC-LUVs showed a less pronounced increase in circulation time (4.3 \pm 0.7 h), suggesting a plateau in the observed effects (Fig. 4C).

Long-term blood retention was comparable for all sterically-stable functionalizations, with $ca.\ 15\pm2$ % of pMPC-LUVs and PEG-LUVs circulating 24 h post-injection (Fig. 4A, B). Organ biodistribution analysis (Fig. 5) revealed similar accumulation trends for both PEG- and pMPC- liposomes, primarily in the spleen and, to a lesser extent, in the liver. Subtle differences were observed with respect to polymer length: PEG liposomes maintained consistent accumulation across different molecular lengths, while pMPC liposomes showed a slight decrease in accumulation with increasing polymer length in both the spleen and liver. These differences suggest that pMPC may regulate liposome uptake by reticuloendothelial-rich tissues in these organs, similar to our observations for cellular uptake.

These results, summarized in Fig. 4 A-D and Fig. S5 point to pMPC polymer molecular weight strongly modulating the blood circulation upon administration - a feature absent with PEGylated carriers, while maintaining an excellent safety profile. This property, combined with the molecular-weight-dependence of cellular uptake regulation, may provide flexibility in selecting an optimal configuration customized for specific applications.

4.4. ABC effect and immunogenicity of repeated administration of pMPC-liposomes in mice

The accelerated blood clearance effect associated with PEGylated liposomes is well documented [41], with numerous studies in animal models demonstrating that the administration of PEGylated liposomes can stimulate the production of antibodies, particularly IgM [78]. This immune response is a critical factor in the ABC phenomenon, as these antibodies promote the rapid clearance of subsequent doses from circulation, primarily through opsonization and complement system activation. This rapid clearance of subsequent doses poses serious challenges associated with the therapeutic use of PEGylated formulations.

We observed a significant reduction in the circulation half-life of PEG-liposomes after the second injection, dropping from approximately

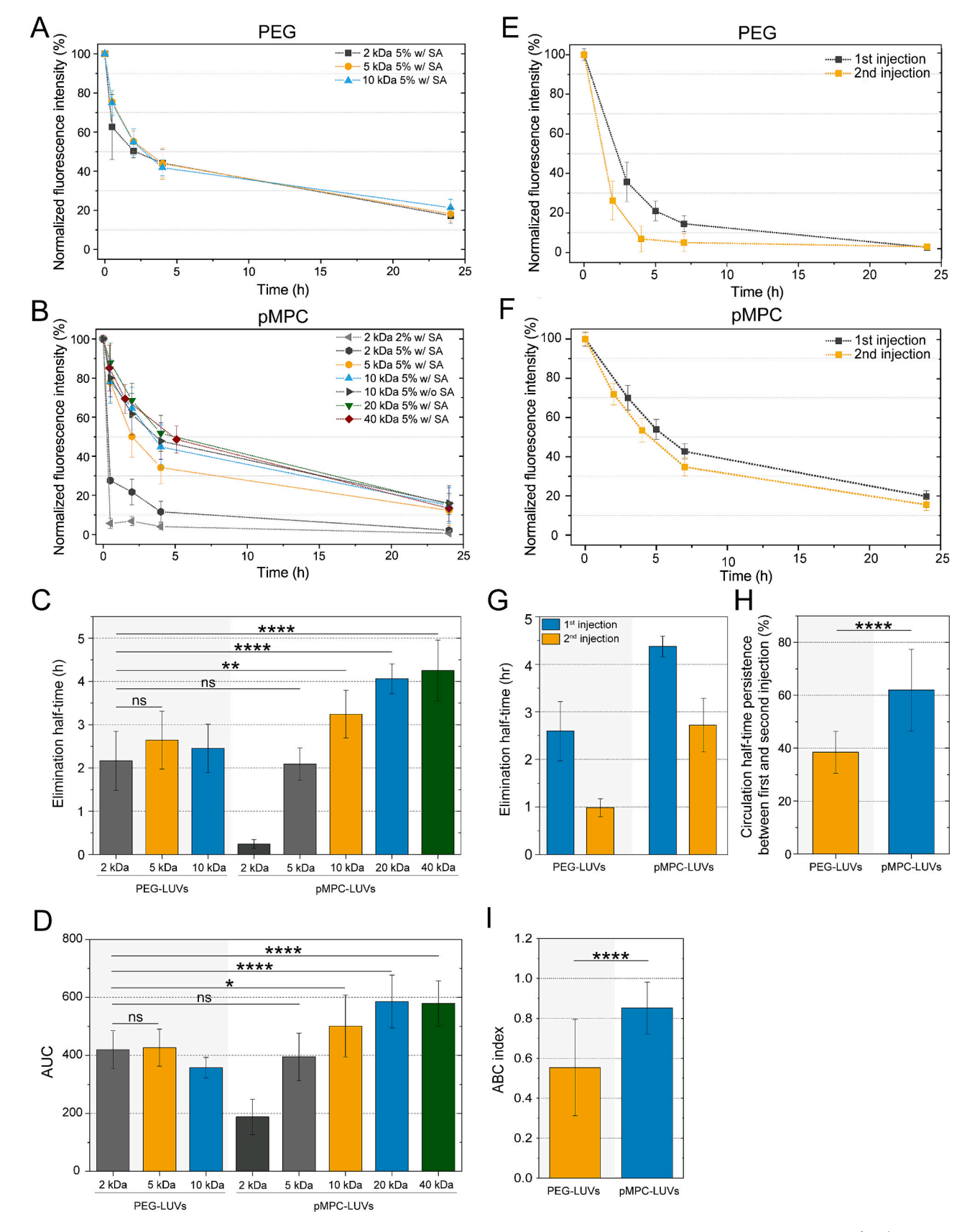
2.6 h to 1 h (a 62 % decrease in blood circulation; see Fig. 4E, G-H). In contrast, pMPC-LUVs showed a less pronounced reduction in blood circulation upon the second injection, decreasing from approximately 4.3 h to about 2.7 h (a 37 % reduction; see Fig. 4F-H). This reduced susceptibility of pMPC-LUVs to ABC suggests they may maintain a more stable pharmacokinetic profile and mitigate immune-mediated side effects associated with repeated administration.

To further investigate the ABC phenomenon, we calculated the ABC index, a quantitative metric used to assess the intensity of the accelerated blood clearance phenomenon, as described by Guo et al. [79]. The ABC index is defined as the ratio of the area under the curve (AUC) versus second dose of liposomes to the AUC of a single dose. According to Guo et al. [79], an ABC index value below 0.9 confirms the occurrence of the ABC phenomenon, indicating enhanced clearance of liposomes upon repeated administration due to immune recognition. Our results (Fig. 41) revealed that pMPC-functionalized liposomes exhibited an ABC index of 0.85 \pm 0.12, suggesting moderate induction of the ABC phenomenon. In contrast, PEG-functionalized liposomes displayed a significantly lower ABC index of 0.55 \pm 0.24, indicating a much more pronounced ABC effect.

The differences in ABC levels can be attributed to the different polymers' physico-chemical properties. The immunogenicity of PEG has been shown to correlate directly with its higher hydrophobicity compared to other polymers [80]. Utilizing the much more hydrophilic pMPC polymer, the ABC phenomenon is inhibited by reducing antibody production, specifically IgM, thereby enhancing the overall effectiveness of the liposomal formulation.

To demonstrate this, we quantified total (*i.e.* non-specific) IgM antibody secretion after a single injection of either PEGylated or pMPCylated liposomes at phospholipid dose (0.05 μ mol phospholipid/kg) [81,82]. Levels of IgM measured five days post-intravenous injection are shown in Fig. 6, with blood serum from mice administered IV PBS alone as a control to establish baseline antibody levels. The control group exhibited an average IgM concentration of 186 μ g/mL, consistent with values reported by the manufacturer and in good agreement with findings by Wang et al. [83]. In line with previous findings, the injection of PEGylated liposomes led to an increased immunoglobulin level, averaging 308 μ g/mL. In contrast, the injection of pMPCylated liposomes provoked a lower immune response, with IgM concentrations measured at 214 μ g/mL - comparable to physiological levels and *ca.* 30 % lower than those of PEGylated liposomes, in agreement with the reduced immunogenicity of pMPC observed by Liang et al. [53].

Our study demonstrates that the lower IgM response associated with pMPC-LUVs contributes to their reduced susceptibility to ABC phenomena. Although pMPCylated carriers show a reduction in circulation time following repeated administration (Fig. 4E and F), this decrease is significantly less pronounced than in PEGylated liposomes. By minimizing the production of antibodies that promote rapid clearance, pMPC-LUVs may offer a more favorable pharmacokinetic profile and lower immunogenicity compared to PEGylated formulations, which in combination with the tunable cellular uptake and blood retention provides a more flexible and customizable functionalization than currently available strategies. These in vivo findings align with the in vitro work of Suzuki et al. [84] and Adler et al., [57] who reported that pMPC-coating inhibits protein adsorption onto liposomes incubated in a mixture of serum proteins (e.g., albumin, complement factors) across various degrees of polymerization, and evade IgM recognition. Adler et al. [57] also demonstrated reduced complement C3 binding in similar experimental in vitro conditions using human plasma, supporting our observation that pMPC-LUVs mitigate the ABC effect through decreased protein interactions. Our assessment of IgM production and the ABC effect in vivo using a murine model both confirm pMPC's immunological advantages, and demonstrates pMPC advantages in a physiologically relevant drug delivery context.



(caption on next page)

Fig. 4. Blood clearance and circulation half-life of DiI-labeled liposomes in CD1 mice. (A, B) Blood clearance profiles of liposomes functionalized with (A) PEG (5 % mol/mol) or (B) pMPC (2 % and 5 % mol/mol) with increasing polymer lengths after a single intravenous (IV) injection and with (w/) or without (w/o) 5 % SA (mol/mol), monitored over 24 h. (C) Blood circulation elimination half-life of PEGylated and pMPCylated liposomes doped with 5 % SA (mol/mol) and with increasing polymer lengths after a single intravenous (IV) injection. (D) area under curve (AUC) of DiI fluorescence fraction calculated from (A) and (B). (E, F) Blood clearance profiles of liposomes doped with 5 % SA (mol/mol) and functionalized with (E) PEG (2 kDa, 5 % mol/mol) or (F) pMPC (20 kDa, 5 % mol/mol) after two IV injections administered 5 days apart. (G) Blood circulation elimination half-life of PEG (2 kDa, 5 % mol/mol) and pMPC (20 kDa, 5 % mol/mol) functionalized liposomes after two IV injections (5 days apart). (H) Percentage change in circulation half-life after the second IV injection (5 days apart) relative to the first for PEG (2 kDa, 5 % mol/mol) and pMPC (20 kDa, 5 % mol/mol) functionalized liposomes. (I) ABC index of PEG (2 kDa, 5 % mol/mol) and pMPC (20 kDa, 5 % mol/mol) – liposomes calculated from (E) and (F). All data are presented as mean \pm SEM, with a minimum of 10 animals per group. Statistical significance: *p < 0.05, **p < 0.01, ****p < 0.001, ****p < 0.001, ****p < 0.001, ****p < 0.001, ****p < 0.0001, ****p < 0.0001, ****p < 0.0001, ****p < 0.0001, ****

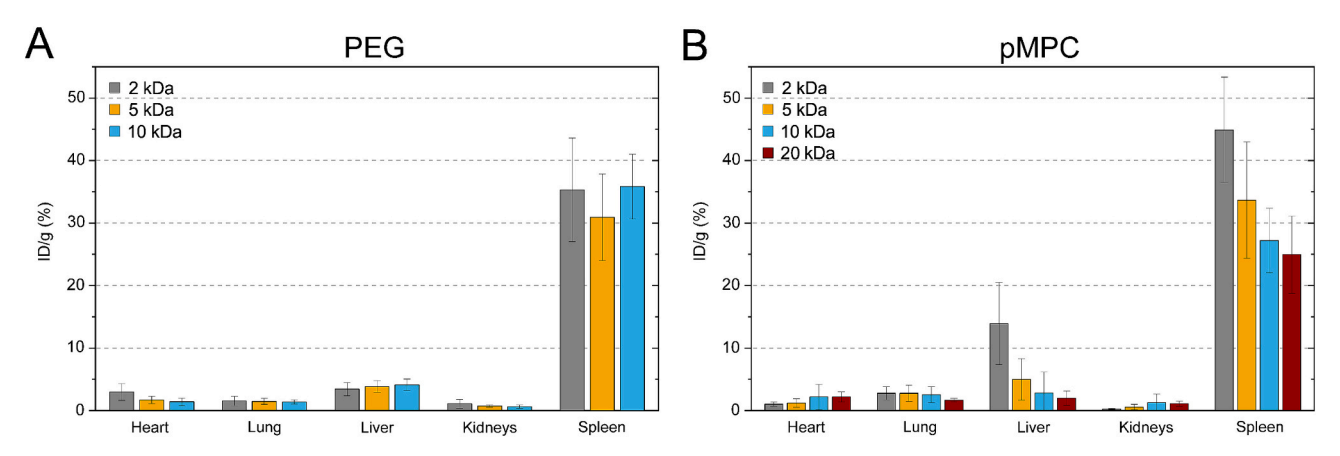


Fig. 5. Quantitative analysis of DiI-labeled liposomes doped with 5 % SA (mol/mol) functionalized with (A) PEG (5 % mol/mol) or (B) pMPC (5 % mol/mol) accumulated in organs 24 h after a single IV injection. Data are presented as mean \pm SEM, with a minimum of 10 animals per group.

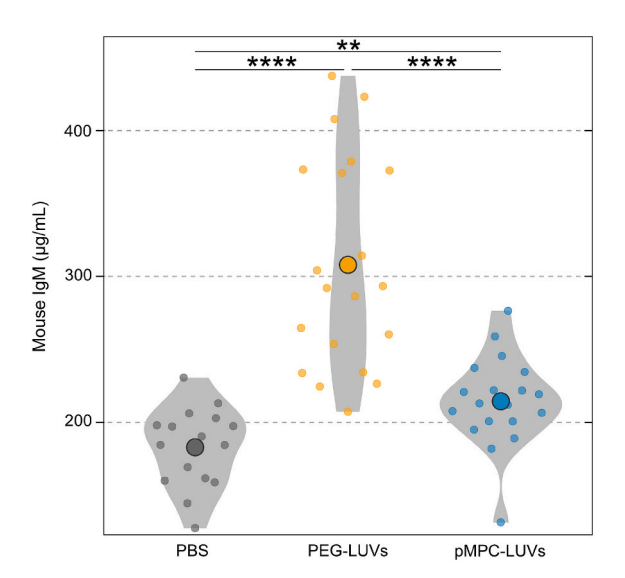


Fig. 6. IgM levels in CD1 mouse blood serum 5 days after IV tail vein injection of 100 μ L PBS or liposomes functionalized with 5 % (mol/mol) PEG (2 kDa) or pMPC (20 kDa), doped with 5 % (mol/mol) SA. Serum IgM levels were measured *via* ELISA kit. Data are presented as a half dot plot aligned in bins and half violin plot to visualize the distribution of data points. Filled circles indicate the median of each dataset. Statistical significance: * p < 0.05, ** p < 0.01, *** p < 0.001, *** p < 0.001, *** p < 0.0001, ns – not significant.

5. Conclusion

Our comprehensive *in vivo* examination of IV-administered pMPC-functionalized liposomes reveals a significant benefit for drug delivery systems, addressing the long-standing limitations of PEGylated formulations. pMPCylated liposomes show high biocompatibility and long-term colloidal stability comparable with PEGylated ones. Under physiological conditions (particularly the presence of serum proteins),

pMPCylation requires a minimum surface coverage and polymer length to provide effective steric repulsion and colloidal stability, which we quantified as 5 % mol/mol with a 5 kDa polymer length as a sufficient coverage to resist protein adsorption. However, pMPC-liposomes display superior performance in key areas – cellular uptake, blood circulation time, the ABC effect and immunogenicity - representing a clear benefit for liposomal drug delivery.

The enhanced cellular uptake observed with pMPC-liposomes, particularly with shorter chain lengths, directly tackles one of the primary drawbacks of PEGylated systems. We found that the cellular uptake of 5 kDa pMPC is about ~5 times higher than 2 kDa PEGylated LUVs, despite the similarity in length of the two polymer moieties. The mechanism behind this enhanced uptake, related to pMPC's unique chemical structure and its interaction with specific cell membrane receptors, providing carriers with a targeting capability. This enhanced uptake potential could significantly improve the efficacy of local treatments requiring targeted drug delivery, potentially enabling more efficient therapeutic outcomes with lower doses and fewer side effects.

Equally significant is the extended circulation time achieved with longer pMPC chains, which significantly surpasses that of PEGliposomes. Moreover, the blood circulation of pMPC-LUVs is markedly affected by polymer length: pMPC functionalization at 5 kDa achieves a circulation half-life of 2 h, comparable to that of PEG-liposomes across all molecular weights studied; however, increasing the pMPC length to 10 kDa results in an elimination half-life of 3.3 h, and 20 kDa and 40 kDa showed even higher values, with elimination half time exceeding 4 h which is 2 times longer than any PEGylated liposomes. This extended circulation time, particularly with longer pMPC chains, could significantly enhance the EPR (enhanced permeability and retention) effect for example, for cancer treatment, allowing greater accumulation of nanocarriers in tumor tissues over time. The enhanced cellular uptake and prolonged blood circulation of pMPC-liposomes not only improve their pharmacokinetic profile but also offer promising potential for targeted accumulation in diseased tissues, such as tumors. While this study establishes the broad advantages of pMPC-liposomes for drug delivery, future research will investigate their efficacy in specific disease

models, including tumor-bearing mice, to explore targeted therapeutic applications. Specifically, comparing the therapeutic efficacy of anticancer agents encapsulated in pMPC-liposomes to conventional PEG carriers in murine cancer models will be crucial to further validate the potential of pMPCylation in therapeutics.

Perhaps most striking is the markedly reduced immunogenicity of pMPC-liposomes compared to their PEGylated counterparts. Two consecutive injections of 20 kDa pMPC-LUVs result in a 37 % decrease in elimination half-life on the second injection, compared to PEGylated liposomes, whose elimination half-time decreases by 62 %. This indicates a lower ABC effect and is in line with the IgM elicitation results which shows a significantly weaker activation of immune response by pMPCylated compared to PEGylated liposomes. The lower IgM response and diminished accelerated blood clearance effect upon repeated administration address an important issue in the clinical application of nanocarriers. This improvement could be particularly relevant for chronic conditions requiring long-term treatment, where the ABC effect has pose a significant obstacle.

In conclusion, our findings position pMPC-functionalized liposomes as a promising alternative to PEGylated formulations, offering a more effective and less immunogenic platform for nanomedicine-based therapies. The customizability of pMPC-liposomes, allowing for modulation of both cellular uptake and circulation time, opens new avenues for tailored treatments, ranging from rapid-acting formulations for acute conditions to long-circulating variants for chronic diseases.

CRediT authorship contribution statement

Monika Kluzek: Writing – review & editing, Writing – original draft, Methodology, Investigation, Conceptualization. Maryana Hamad: Writing – review & editing, Methodology, Investigation. Weifeng Lin: Writing – review & editing, Methodology, Investigation, Conceptualization. Evgenia Mitsou: Writing – review & editing, Methodology, Investigation. Ziv Porat: Writing – review & editing, Methodology, Investigation. Yuri Kuznetsov: Writing – review & editing, Methodology, Investigation. Yaara Oppenheimer-Shaanan: Writing – review & editing, Methodology, Investigation, Conceptualization. Jacob Klein: Writing – review & editing, Writing – original draft, Validation, Supervision, Project administration, Methodology, Investigation, Funding acquisition, Conceptualization.

Ethical statements

All procedures on animals were approved by IACUC committee (no. 03870520-2, no. 04200522-1 and no. 02900322-2).

Funding

Israel Ministry of Science and Industry (grant 713272); Israel Science Foundation-National Science Foundation China joint program (grant ISF-NSFC 2577/17); European Research Council (ERC) under the European Union's Horizon 2020 research and innovation programme (grant agreement No. 743016); European Research Council Proof-of-Concept (PoC) programme (NanodeliveryEnhance project number: 101082135); National Science Centre, Poland (NCN OPUS26, grant 2023/51/B/NZ7/01177).

Declaration of competing interest

The authors declare the following competing financial interest(s): Yeda Research and Development Co. LTD at the Weizmann Institute of Science has a patent on pMPC-lipid conjugation methodology (US10730976B2).

Acknowledgements

This work was made possible in part by the historic generosity of the Harold Perlman family. We would like to thank Dr. Yoav Barak from Department of Chemical Research Support (BioNANO lab) for microplate reader measurement assistance (Weizmann Institute of Science). We would like to also thank Veronica Frydman for providing the pMPC-conjugated lipids. Nanosight NTA measurements were done at the Protein Analysis Unit (Weizmann Institute of Science). Dynamic light scattering (DLS) measurements were perform at Chemical Research Support unit (Weizmann Institute of Science). E.M. would like to thank the Azrieli Foundation for the International Postdoctoral Fellowship (2022-2025). Graphical abstract was created using Biorender platform (www.biorender.com).

Appendix A. Supplementary data

Supplementary data to this article can be found online at https://doi.org/10.1016/j.jconrel.2025.114306.

Data availability

All data supporting this study are available in the manuscript and supplementary materials.

References

- L. Sun, H. Liu, Y. Ye, Y. Lei, R. Islam, S. Tan, et al., Smart nanoparticles for cancer therapy, Signal Transduct. Target. Ther. 8 (2023) 418, https://doi.org/10.1038/ s41392-023-01642-x.
- [2] W. Xiu, J. Shan, K. Yang, H. Xiao, L. Yuwen, L. Wang, Recent development of nanomedicine for the treatment of bacterial biofilm infections, View 2 (2021) 20200065, https://doi.org/10.1002/viw.20200065.
- [3] R. Tenchov, R. Bird, A.E. Curtze, Q. Zhou, Lipid nanoparticles from liposomes to mRNA vaccine delivery, a landscape of research diversity and advancement, ACS Nano 15 (2021) 16982–17015, https://doi.org/10.1021/acsnano.1c04996.
- [4] M.J. Mitchell, M.M. Billingsley, R.M. Haley, M.E. Wechsler, N.A. Peppas, R. Langer, Engineering precision nanoparticles for drug delivery, Nat. Rev. Drug Discov. 20 (2021) 101–124, https://doi.org/10.1038/s41573-020-0090-8.
- [5] J. Wolfram, M. Ferrari, Clinical cancer nanomedicine, Nano Today 25 (2019) 85–98, https://doi.org/10.1016/j.nantod.2019.02.005.
- [6] K.-W. Huang, F.-F. Hsu, J.T. Qiu, G.-J. Chern, Y.-A. Lee, C.-C. Chang, et al., Highly efficient and tumor-selective nanoparticles for dual-targeted immunogene therapy against cancer, Sci. Adv. 6 (2020) eaax5032, https://doi.org/10.1126/sciadv.aax5032.
- [7] D. Li, X. Wei, W. Xue, L. Xu, Z. Xiang, S. Liu, et al., Size effect of Zwitterionic peptide-based nanoscale micelles on cancer therapy, ACS Appl. Nano Mater. 5 (2022) 9344–9355, https://doi.org/10.1021/acsanm.2c01665.
- [8] A.M.D.S. Jayawardhana, Z. Qiu, S. Kempf, H. Wang, M. Miterko, D.J. Bowers, et al., Dual-action organoplatinum polymeric nanoparticles overcoming drug resistance in ovarian cancer, Dalton T 48 (2019) 12451–12458, https://doi.org/10.1039/c9dt01683j.
- [9] M.A. Beach, U. Nayanathara, Y. Gao, C. Zhang, Y. Xiong, Y. Wang, et al., Polymeric nanoparticles for drug delivery, Chem. Rev. 124 (2024) 5505–5616, https://doi. org/10.1021/acs.chemrev.3c00705.
- [10] X. Wei, Z. Xiang, W. Xue, S. Chen, Enhancing the antitumor efficacy of Zwitterionic peptide-based nanoscale micelles through sensitizing their response in solid tumors, ACS Appl. Nano Mater. 5 (2022) 16942–16954, https://doi.org/10.1021/ acsanm.2c03880.
- [11] N. Habibi, A. Mauser, Y. Ko, J. Lahann, Protein nanoparticles: uniting the power of proteins with engineering design approaches, Adv. Sci. 9 (2022) 2104012, https://doi.org/10.1002/advs.202104012.
- [12] H. Sun, X. Guo, S. Zeng, Y. Wang, J. Hou, D. Yang, et al., A multifunctional liposomal nanoplatform co-delivering hydrophobic and hydrophilic doxorubicin for complete eradication of xenografted tumors, Nanoscale 11 (2019) 17759–17772, https://doi.org/10.1039/c9nr04669k.
- [13] T. Peng, W. Xu, Q. Li, Y. Ding, Y. Huang, Pharmaceutical liposomal delivery—specific considerations of innovation and challenges, Biomater. Sci. 11 (2022) 62–75, https://doi.org/10.1039/d2bm01252a.
- [14] C. Ochoa-Sánchez, E. Rodríguez-León, R. Iñiguez-Palomares, C. Rodríguez-Beas, Brief comparison of the efficacy of cationic and anionic liposomes as nonviral delivery systems, ACS Omega 9 (2024) 46664–46678, https://doi.org/10.1021/ acsomega.4c06714.
- [15] H. Wang, S. Lin, X. Wu, K. Jiang, H. Lu, C. Zhan, Interplay between liposomes and IgM: principles, challenges, and opportunities, Adv. Sci. 10 (2023) 2301777, https://doi.org/10.1002/advs.202301777.
- [16] F. Giulimondi, L. Digiacomo, D. Pozzi, S. Palchetti, E. Vulpis, A.L. Capriotti, et al., Interplay of protein corona and immune cells controls blood residency of

- liposomes, Nat. Commun. 10 (2019) 3686, https://doi.org/10.1038/s41467-019-11642.7
- [17] C. Pavón, E.M. Benetti, F. Lorandi, Polymer brushes on nanoparticles for controlling the interaction with protein-rich physiological media, Langmuir 40 (2024) 11843–11857, https://doi.org/10.1021/acs.langmuir.4c00956.
- [18] M. Mahmoudi, M.P. Landry, A. Moore, R. Coreas, The protein corona from nanomedicine to environmental science, Nat. Rev. Mater. 8 (2023) 422–438, https://doi.org/10.1038/s41578-023-00552-2.
- [19] J.R. Shaw, N. Caprio, N. Truong, M. Weldemariam, A. Tran, N. Pilli, et al., Inflammatory disease progression shapes nanoparticle biomolecular coronamediated immune activation profiles, Nat. Commun. 16 (2025) 924, https://doi. org/10.1038/s41467-025-56210-4.
- [20] A. Arcella, S. Palchetti, L. Digiacomo, D. Pozzi, A.L. Capriotti, L. Frati, et al., Brain targeting by liposome-biomolecular corona boosts anticancer efficacy of temozolomide in glioblastoma cells, ACS Chem. Neurosci. 9 (2018) 3166–3174, https://doi.org/10.1021/acschemneuro.8b00339.
- [21] J. Bourquin, A. Milosevic, D. Hauser, R. Lehner, F. Blank, A. Petri-Fink, et al., Biodistribution, clearance, and long-term fate of clinically relevant nanomaterials, Adv. Mater. 30 (2018) e1704307, https://doi.org/10.1002/adma.201704307.
- [22] Y. Li, R. Yao, M. Ren, K. Yuan, Y. Du, Y. He, et al., Liposomes trigger bone marrow niche macrophage "foam" cell formation and affect hematopoiesis in mice, J. Lipid Res. 63 (2022) 100273, https://doi.org/10.1016/j.jlr.2022.100273.
- [23] W. Poon, B.R. Kingston, B. Ouyang, W. Ngo, W.C.W. Chan, A framework for designing delivery systems, Nat. Nanotechnol. 15 (2020) 819–829, https://doi. org/10.1038/s41565-020-0759-5.
- [24] A.M. López-Estevez, R. Gref, M.J. Alonso, A journey through the history of PEGylated drug delivery nanocarriers, Drug Deliv. Transl. Res. 14 (2024) 2026–2031, https://doi.org/10.1007/s13346-024-01608-8.
- [25] S. Zalba, T.L.M. ten Hagen, C. Burgui, M.J. Garrido, Stealth nanoparticles in oncology: facing the PEG dilemma, J. Control. Release 351 (2022) 22–36, https:// doi.org/10.1016/j.jconrel.2022.09.002.
- [26] R. Münter, C. Stavnsbjerg, E. Christensen, M.E. Thomsen, A. Stensballe, A. E. Hansen, et al., Unravelling heterogeneities in complement and antibody opsonization of individual liposomes as a function of surface architecture, Small 18 (2022) e2106529, https://doi.org/10.1002/smll.202106529.
- [27] M.F.S. Deuker, V. Mailänder, S. Morsbach, K. Landfester, Anti-PEG antibodies enriched in the protein corona of PEGylated nanocarriers impact the cell uptake, Nanoscale Horiz. 8 (2023) 1377–1385, https://doi.org/10.1039/d3nh00198a.
- [28] J.S. Suk, Q. Xu, N. Kim, J. Hanes, L.M. Ensign, PEGylation as a strategy for improving nanoparticle-based drug and gene delivery, Adv. Drug Deliv. Rev. 99 (2016) 28–51. https://doi.org/10.1016/j.addr.2015.09.012
- (2016) 28–51, https://doi.org/10.1016/j.addr.2015.09.012.
 [29] Y. Takakura, Y. Takahashi, Strategies for persistent retention of macromolecules and nanoparticles in the blood circulation, J. Control. Release 350 (2022) 486–493, https://doi.org/10.1016/j.jconrel.2022.05.063.
- [30] E. Beltrán-Gracia, A. López-Camacho, I. Higuera-Ciapara, J.B. Velázquez-Fernández, A.A. Vallejo-Cardona, Nanomedicine review: clinical developments in liposomal applications, Cancer Nanotechnol. 10 (2019) 11, https://doi.org/10.1186/s12645-019-0055-v.
- [31] M. de Bourayne, S. Meunier, S. Bitoun, E. Correia, X. Mariette, H. Nozach, et al., Pegylation reduces the uptake of Certolizumab Pegol by dendritic cells and epitope presentation to T-cells, Front. Immunol. 13 (2022) 808606, https://doi.org/ 10.3389/fimmu.2022.808606.
- [32] D. Stengel, B.H. Demirel, P. Knoll, M. Truszkowska, F. Laffleur, A. Bernkop-Schnürch, PEG vs. zwitterions: how these surface decorations determine cellular uptake of lipid-based nanocarriers, J. Colloid Interface Sci. 647 (2023) 52–64, https://doi.org/10.1016/j.jcis.2023.05.079.
- [33] M. Li, S. Jiang, J. Simon, D. Paßlick, M.-L. Frey, M. Wagner, et al., Brush conformation of polyethylene glycol determines the stealth effect of nanocarriers in the low protein adsorption regime, Nano Lett. 21 (2021) 1591–1598, https://doi.org/10.1021/acs.nanolett.0c03756.
- [34] N. d'Avanzo, C. Celia, A. Barone, M. Carafa, L.D. Marzio, H.A. Santos, et al., Immunogenicity of polyethylene glycol based nanomedicines: mechanisms, clinical implications and systematic approach, Adv. Ther. 3 (2020) 1900170, https://doi. org/10.1002/adtp.201900170.
- [35] G. Kozma, T. Shimizu, T. Ishida, J. Szebeni, Anti-PEG antibodies: properties, formation and role in adverse immune reactions to PEGylated nanobiopharmaceuticals, Adv. Drug Deliv. Rev. 154–155 (2020) 163–175, https://doi.org/10.1016/j.addr.2020.07.024.
- [36] T. Suzuki, Y. Suzuki, T. Hihara, K. Kubara, K. Kondo, K. Hyodo, et al., PEG shedding-rate-dependent blood clearance of PEGylated lipid nanoparticles in mice: faster PEG shedding attenuates anti-PEG IgM production, Int. J. Pharm. 588 (2020) 119792. https://doi.org/10.1016/j.jinharm.2020.119792
- 119792, https://doi.org/10.1016/j.ijpharm.2020.119792.
 [37] B.-M. Chen, T.-L. Cheng, S.R. Roffler, Polyethylene glycol immunogenicity: theoretical, clinical, and practical aspects of anti-polyethylene glycol antibodies, ACS Nano 15 (2021) 14022–14048, https://doi.org/10.1021/acsnano.1c05922.
- [38] A. Gabizon, J. Szebeni, Complement activation: a potential threat on the safety of poly(ethylene glycol)-coated nanomedicines, ACS Nano 14 (2020) 7682–7688, https://doi.org/10.1021/acsnano.0c03648.
- [39] G.T. Kozma, T. Mészáros, I. Vashegyi, T. Fülöp, E. Örfi, L. Dézsi, et al., Pseudo-anaphylaxis to polyethylene glycol (PEG)-coated liposomes: roles of anti-PEG IgM and complement activation in a porcine model of human infusion reactions, ACS Nano 13 (2019) 9315–9324, https://doi.org/10.1021/acsnano.9b03942.
- [40] C. Stavnsbjerg, E. Christensen, R. Münter, J.R. Henriksen, M. Fach, L. Parhamifar, et al., Accelerated blood clearance and hypersensitivity by PEGylated liposomes containing TLR agonists, J. Control. Release 342 (2022) 337–344, https://doi.org/10.1016/j.jconrel.2021.12.033.

- [41] M. Mohamed, A.S.A. Lila, T. Shimizu, E. Alaaeldin, A. Hussein, H.A. Sarhan, et al., PEGylated liposomes: immunological responses, Sci. Technol. Adv. Mater. 20 (2019) 710–724, https://doi.org/10.1080/14686996.2019.1627174.
- [42] G. Liang, W. Ma, Y. Zhao, E. Liu, X. Shan, W. Ma, et al., Risk factors for pegylated liposomal doxorubicin-induced moderate to severe hand-foot syndrome in breast cancer patients: assessment of baseline clinical parameters, BMC Cancer 21 (2021) 362, https://doi.org/10.1186/s12885-021-08028-8.
- [43] W.-A. Chen, D.-Y. Chang, B.-M. Chen, Y.-C. Lin, Y. Barenholz, S.R. Roffler, Antibodies against poly(ethylene glycol) activate innate immune cells and induce hypersensitivity reactions to PEGylated nanomedicines, ACS Nano 17 (2023) 5757–5772, https://doi.org/10.1021/acsnano.2c12193.
- [44] Q. Yang, T.M. Jacobs, J.D. McCallen, D.T. Moore, J.T. Huckaby, J.N. Edelstein, et al., Analysis of pre-existing IgG and IgM antibodies against polyethylene glycol (PEG) in the general population, Anal. Chem. 88 (2016) 11804–11812, https://doi.org/10.1021/acs.analchem.6b03437.
- [45] Q. Li, C. Wen, J. Yang, X. Zhou, Y. Zhu, J. Zheng, et al., Zwitterionic biomaterials, Chem. Rev. 122 (2022) 17073–17154, https://doi.org/10.1021/acs. chemrev.2c00344.
- [46] Y. Li, R. Liu, Y. Shi, Z. Zhang, X. Zhang, Zwitterionic poly(carboxybetaine)-based cationic liposomes for effective delivery of small interfering RNA therapeutics without accelerated blood clearance phenomenon, Theranostics 5 (2015) 583–596, https://doi.org/10.7150/thno.11234.
- [47] Y. Tian, H. Lv, Y. Ju, J. Hao, J. Cui, Zwitterionic poly(ethylene glycol) nanoparticles minimize protein adsorption and immunogenicity for improved biological fate, ACS Appl. Mater. Interfaces 17 (2025) 6125–6133, https://doi.org/ 10.1021/acsami.4c20890.
- [48] T. Ryujin, T. Shimizu, R. Miyahara, D. Asai, R. Shimazui, T. Yoshikawa, et al., Blood retention and antigenicity of polycarboxybetaine-modified liposomes, Int. J. Pharm. 586 (2020) 119521, https://doi.org/10.1016/j.ijpharm.2020.119521.
- [49] A. Erfani, J. Seaberg, C.P. Aichele, J.D. Ramsey, Interactions between biomolecules and Zwitterionic moieties: a review, Biomacromolecules 21 (2020) 2557–2573, https://doi.org/10.1021/acs.biomac.0c00497.
- [50] S. Moayedi, W. Xia, L. Lundergan, H. Yuan, J. Xu, Zwitterionic polymers for biomedical applications: antimicrobial and antifouling strategies toward implantable medical devices and drug delivery, Langmuir 40 (2024) 23125–23145, https://doi.org/10.1021/acs.langmuir.4c02664.
- [51] W. Lin, R. Goldberg, J. Klein, Poly-phosphocholination of liposomes leads to highly-extended retention time in mice joints, J. Mater. Chem. B (2022), https://doi.org/10.1039/d1tb02346b.
- [52] W. Lin, N. Kampf, R. Goldberg, M.J. Driver, J. Klein, Poly-phosphocholinated liposomes form stable superlubrication vectors, Langmuir 35 (2019) 6048–6054, https://doi.org/10.1021/acs.langmuir.9b00610.
- [53] S. Liang, Y. Liu, X. Jin, G. Liu, J. Wen, L. Zhang, et al., Phosphorylcholine polymer nanocapsules prolong the circulation time and reduce the immunogenicity of therapeutic proteins, Nano Res 9 (2016) 1022–1031, https://doi.org/10.1007/ s12274_016_0901_3
- [54] S. Cho, M. Hori, R. Ueki, Y. Saito, Y. Nagai, H. Iki, et al., Zwitterionic polymer with minimal reactivity against PEG antibodies to enhance the therapeutic effects of cytokine-targeting DNA aptamer, Biomater. Sci. 13 (2025) 1347–1353, https://doi. org/10.1039/d4bm01541j.
- [55] K. Ishihara, Revolutionary advances in 2-methacryloyloxyethyl phosphorylcholine polymers as biomaterials, J. Biomed. Mater. Res. Part A 107 (2019) 933–943, https://doi.org/10.1002/jbm.a.36635.
- [56] K. Ishihara, Blood-compatible surfaces with phosphorylcholine-based polymers for cardiovascular medical devices, Langmuir 35 (2019) 1778–1787, https://doi.org/ 10.1021/acs.langmuir.8b01565.
- [57] A. Adler, Y. Inoue, K.N. Ekdahl, T. Baba, K. Ishihara, B. Nilsson, et al., Effect of liposome surface modification with water-soluble phospholipid polymer chainconjugated lipids on interaction with human plasma proteins, J. Mater. Chem. B (2021), https://doi.org/10.1039/d1tb01485d.
- [58] L. Zhu, W. Lin, M. Kluzek, J. Miotla-Zarebska, V. Batchelor, M. Gardiner, et al., Liposomic lubricants suppress acute inflammatory gene regulation in the joint in vivo, Acta Biomater. 198 (2025) 366–376, https://doi.org/10.1016/j. arthip.2025.04.022
- [59] M. Kluzek, Y. Oppenheimer-Shaanan, T. Dadosh, M.I. Morandi, O. Avinoam, C. Raanan, et al., Designer Liposomic Nanocarriers are effective biofilm eradicators, ACS Nano (2022), https://doi.org/10.1021/acsnano.2c04232.
- [60] B.-M. Chen, E. Chen, Y.-C. Lin, T.T.M. Tran, K. Turjeman, S.-H. Yang, et al., Liposomes with low levels of grafted poly(ethylene glycol) remain susceptible to destabilization by anti-poly(ethylene glycol) antibodies, ACS Nano 18 (2024) 22122–22138, https://doi.org/10.1021/acsnano.4c05409.
- [61] F. Mastrotto, C. Brazzale, F. Bellato, S.D. Martin, G. Grange, M. Mahmoudzadeh, et al., In vitro and in vivo behavior of liposomes decorated with PEGs with different chemical features, Mol. Pharm. 17 (2020) 472–487, https://doi.org/10.1021/acs. molpharmaceut.9b00887.
- [62] E. Triantafyllopoulou, N. Pippa, C. Demetzos, Protein-liposome interactions: the impact of surface charge and fluidisation effect on protein binding, J. Liposome Res. (2022) 1–12, https://doi.org/10.1080/08982104.2022.2071296.
- [63] N.M. La-Beck, MdR Islam, M.M. Markiewski, Nanoparticle-induced complement activation: implications for cancer nanomedicine, Front. Immunol. 11 (2021) 603039, https://doi.org/10.3389/fimmu.2020.603039.
- [64] J.B. Schlenoff, Zwitteration: coating surfaces with Zwitterionic functionality to reduce nonspecific adsorption, Langmuir 30 (2014) 9625–9636, https://doi.org/ 10.1021/1500057i
- [65] S.A. Tolba, W. Xia, Molecular insights into the hydration of zwitterionic polymers, Mol. Syst. Des. Eng. 8 (2023) 1040–1048, https://doi.org/10.1039/d3me00020f.

- [66] A. Adler, Y. Inoue, Y. Sato, K. Ishihara, K.N. Ekdahl, B. Nilsson, et al., Synthesis of poly(2-methacryloyloxyethyl phosphorylcholine)-conjugated lipids and their characterization and surface properties of modified liposomes for protein interactions, Biomater. Sci.-Uk 9 (2021) 5854–5867, https://doi.org/10.1039/ dlbm00570g
- [67] E. Mantlo, N. Bukreyeva, J. Maruyama, S. Paessler, C. Huang, Potent antiviral activities of type I interferons to SARS-CoV-2 infection, Biorxiv (2020), https://doi. org/10.1101/2020.04.02.022764, 2020.04.02.022764.
- [68] R.C. Puerari, E. Ferrari, M.G. de Cezar, R.A. Gonçalves, C. Simioni, L.C. Ouriques, et al., Investigation of toxicological effects of amorphous silica nanostructures with amine-functionalized surfaces on Vero cells, Chemosphere 214 (2019) 679–687, https://doi.org/10.1016/j.chemosphere.2018.09.165.
- [69] S. Eash, W. Querbes, W.J. Atwood, Infection of Vero cells by BK virus is dependent on Caveolae, J. Virol. 78 (2004) 11583–11590, https://doi.org/10.1128/ ivi.78.21.11583-11590.2004.
- [70] J. Rodríguez, J. Mosquera, J.R. Couceiro, J.R. Nitschke, M.E. Vázquez, J. L. Mascareñas, Anion recognition as a supramolecular switch of cell internalization, J. Am. Chem. Soc. 139 (2017) 55–58, https://doi.org/10.1021/jacs.6b11103.
- [71] J.D. Torres-Vanegas, J. Cifuentes, P.R. Puentes, V. Quezada, A.J. Garcia-Brand, J. C. Cruz, et al., Assessing cellular internalization and endosomal escape abilities of novel BUFII-graphene oxide nanobioconjugates, Front. Chem. 10 (2022) 974218, https://doi.org/10.3389/fchem.2022.974218.
- [72] J. Grundler, K. Shin, H.-W. Suh, M. Zhong, W.M. Saltzman, Surface topography of polyethylene glycol shell nanoparticles formed from bottlebrush block copolymers controls interactions with proteins and cells, ACS Nano 15 (2021) 16118–16129, https://doi.org/10.1021/acsnano.1c04835.
- [73] C.E. de Castro, C.A.S. Ribeiro, A.C. Alavarse, L.J.C. Albuquerque, da Silva MCC, E. Jäger, et al., Nanoparticle-cell interactions: surface chemistry effects on the cellular uptake of biocompatible block copolymer assemblies, Langmuir 34 (2018) 2180–2188, https://doi.org/10.1021/acs.langmuir.7b04040.
- [74] H.E. Colley, V. Hearnden, M. Avila-Olias, D. Cecchin, I. Canton, J. Madsen, et al., Polymersome-mediated delivery of combination anticancer therapy to head and

- neck cancer cells: 2D and 3D in vitro evaluation, Mol. Pharm. 11 (2014) 1176–1188, https://doi.org/10.1021/mp400610b.
- [75] F. Fenaroli, J.D. Robertson, E. Scarpa, V.M. Gouveia, C.D. Guglielmo, C.D. Pace, et al., Polymersomes eradicating intracellular bacteria, ACS Nano 14 (2020) 8287–8298, https://doi.org/10.1021/acsnano.0c01870.
- [76] S. Acosta-Gutiérrez, D. Matias, M. Avila-Olias, V.M. Gouveia, E. Scarpa, J. Forth, et al., A multiscale study of phosphorylcholine driven cellular phenotypic targeting, Acs Central Sci. 8 (2022) 891–904, https://doi.org/10.1021/acscentsci.2c00146.
- [77] H.-S. Lim, Y.S. Seo, S.M. Ryu, B.C. Moon, G. Choi, J.-S. Kim, Two-week repeated oral dose toxicity study of Mantidis Ootheca water extract in C57BL/6 mice, Évid-Based Complement. Altern. Med. 2019 (2019) 6180236, https://doi.org/10.1155/ 2019/6180236.
- [78] K. Jiang, K. Tian, Y. Yu, E. Wu, M. Yang, F. Pan, et al., Kupffer cells determine intrahepatic traffic of PEGylated liposomal doxorubicin, Nat. Commun. 15 (2024) 6136, https://doi.org/10.1038/s41467-024-50568-7.
- [79] C. Guo, H. Yuan, Y. Wang, Y. Feng, Y. Zhang, T. Yin, et al., The interplay between PEGylated nanoparticles and blood immune system, Adv. Drug Deliv. Rev. 200 (2023) 115044, https://doi.org/10.1016/j.addr.2023.115044.
- [80] Z. Yuan, P. McMullen, S. Luozhong, P. Sarker, C. Tang, T. Wei, et al., Hidden hydrophobicity impacts polymer immunogenicity, Chem. Sci. 14 (2023) 2033–2039, https://doi.org/10.1039/d2sc07047b.
- [81] M. Ichihara, T. Shimizu, A. Imoto, Y. Hashiguchi, Y. Uehara, T. Ishida, et al., Anti-PEG IgM response against PEGylated liposomes in mice and rats, Pharm 3 (2010) 1–11, https://doi.org/10.3390/pharmaceutics3010001.
- [82] T. Ishida, X. Wang, T. Shimizu, K. Nawata, H. Kiwada, PEGylated liposomes elicit an anti-PEG IgM response in a T cell-independent manner, J. Control. Release 122 (2007) 349–355, https://doi.org/10.1016/j.jconrel.2007.05.015.
- [83] J. Wang, J. Yu, Y. Zhang, X. Zhang, A.R. Kahkoska, G. Chen, et al., Charge-switchable polymeric complex for glucose-responsive insulin delivery in mice and pigs, Sci. Adv. 5 (2019) eaaw4357, https://doi.org/10.1126/sciadv.aaw4357.
- [84] H. Suzuki, A. Adler, T. Huang, A. Kuramochi, Y. Ohba, Y. Sato, et al., Impact of spontaneous liposome modification with phospholipid polymer-lipid conjugates on protein interactions, Sci. Technol. Adv. Mater. 23 (2022) 845–857, https://doi. org/10.1080/14686996.2022.2146466.